J Mater Sci: Mater Electron (2021) 32:133–140

Influence of Cu and Ni dopants on the sensing properties of ZnO gas sensor

R. Herrera-Rivera[1,*], J. Morales-Bautista[2], Ana María Pineda-Reyes[2], H. Rojas-Chávez[3], A. Maldonado[2,4], H. Vilchis[1], F. Montejo-Alvaro[5], M. G. Salinas-Juárez[6], and M. de la L. Olvera[2,4,*]

[1] *Instituto de Investigación e Innovación en Energías Renovables, Universidad de Ciencias y Artes de Chiapas, Libramiento Norte Poniente 1150, Col. Lajas Maciel, 29035 Tuxtla Gutiérrez, Chiapas, Mexico*

[2] *Programa de Doctorado en Nanociencias y Nanotecnología, Centro de Investigación y de Estudios Avanzados del Instituto Politécnico Nacional, Av Instituto Politécnico Nacional 2508, San Pedro Zacatenco, Gustavo A. Madero, 07360 Mexico, Mexico*

[3] *Tecnologico Nacional de Mexico, Instituto Tecnologico de Tlahuac II, Camino Real 625, Col. Jardines del Llano, San Juan Ixtayopan. Alcaldía Tláhuac, 13508 Mexico, Mexico*

[4] *Departamento de Ingeniería Eléctrica-SEES, Centro de Investigación y de Estudios Avanzados del Instituto Politécnico Nacional, Av Instituto Politécnico Nacional 2508, San Pedro Zacatenco, Gustavo A. Madero, 07360 Mexico, Mexico*

[5] *Universidad Tecnológica de La Mixteca, Carretera a Acatlima Km. 2.5, Acatlima, 69000 Huajuapan de León, Oaxaca, Mexico*

[6] *Facultad de Estudios Superiores Zaragoza, Campus II, Universidad Nacional Autónoma de México, Batalla 5 de Mayo s/n Esquina Fuerte de Loreto, Col. Ejército de Oriente, Iztapalapa, 09230 Mexico, Mexico*

Received: 16 October 2019
Accepted: 20 October 2020
Published online: 5 November 2020

ABSTRACT

In this work, the influence of Cu and Ni doping on the propane gas (C_3H_8) detection of zinc oxide (ZnO) samples was evaluated. Three powder samples: (a) pure ZnO, (b) Ni-doped ZnO, and (c) Cu-doped ZnO, were obtained by homogenous precipitation method. The Ni and Cu concentration was of 1 at.%. The X-ray diffractograms indicate that all samples showed a hexagonal wurtzite-type crystal structure. Micrographs obtained by scanning electron microscopy (SEM) show a spherical surface morphology typical of nanostructured materials in the pure ZnO and ZnO/Ni samples. The gas sensing devices were manufactured by pressing the powders in pellets form. The sensing response of all pellets was measured by the surface electrical resistance change in a propane (C_3H_8) atmosphere at concentrations from 0 to 500 ppm at different operation temperatures (100, 200, and 300 °C). ZnO/Cu pellet presented the highest resistance change, registered at 300 °C in a propane concentration of 500 ppm.

Address correspondence to E-mail: sharol4@hotmail.com; molvera@cinvestav.mx

https://doi.org/10.1007/s10854-020-04725-5

1 Introduction

It is well known that many dangerous substances are emitted into the atmosphere, mainly due to industrial activity and the accelerated urbanization in the last decades [1–3]; hence, the use of gas sensors to detect and monitor these substances is essential [3]. Studies on gas sensors based on metal oxide semiconductors (MOS) researches, specifically chemical sensors, play an important role in the development of sensing devices used for controlling the toxic gases in the environment [4], that is why in recent years, there has been an increase in the development of sensors with high performance in their response magnitude and selectivity; additionally, a low manufacturing cost [1, 5–7]. There is currently a wide range of MOS used in the field of gas sensors, for example: ZnO [8], TiO_2 [6–9], SnO_2 [10], $MgSb_2O_6$ [11], $ZnMn_2O_4$ [12], V_2O_5 [13], CuO [14], and $CuFe_2O_4$ [15], among others. Among the oxides mentioned above, ZnO is one of the most widely studied, since it exhibits a wide variety of morphologies which are beneficial for gas sensing applications; among the nanostructures reported, we can mention nanoflowers [16], nanorods [17], nanowires [18], and nanosheets [19]. It has been reported that some of the mentioned nanostructures favor the sensitivity and response speed to the analyte gas as compared to the structures in flat thin films and bulk materials; this is due to higher surface–volume ratio. Therefore, materials with high surface area are potentially promising for gas sensors [1, 2, 5]. Furthermore, the specific surface area is increased in smaller particles, which in turn improves the gas detection performance; in this respect, it has been stated that the sensitivity magnitude depends partially on the shape and dimensions of particles [7, 20].

ZnO has been studied in its various structures, such as nanorods used in gas sensors to detect ethanol, with a high reversible and rapid response to reducing ethanol [3, 7]. Nanotubes used to detect nitrogen dioxide, showing excellent detection capacity with a response of 500 ppm at 30 °C [21]. Nanowires were manufactured for interaction with various gas environments, identifying a significant influence on the detection of carbon monoxide, and [20] highly sensitive gas sensors in ethanol detection [22]. Nanoparticles were connected to each other forming ZnO chains for the detection of NO_2, H_2 and CH_4, reflecting a high and reversible response in chemical sensors [23].

Another strategy commonly used in the design MOS, particularly in ZnO, gas sensors is through the doping. For example, authors such as Diaz et al. [2] evaluated the reducing effect of H_2 and CO, doping the ZnO with Au nanoparticles, obtaining a high response to H_2 gas but poor response to CO. Dilonardo et al. [3] investigated the influence of ZnO doping with Au nanoparticles, finding a significantly better detection response of NO_2 compared to non-doped sensors. Ganbayle et al. [24] analyzed Ni-doped ZnO gas sensors, showing excellent detection capacity and improved selectivity. Deshwal and Arora [25] reported a study of ZnO acetone sensors doped with Au, detecting a very high sensitivity of fast response and short recovery times, in contrast with undoped ZnO. However, so far, most studies have been focused on ZnO thin films doped with elements of the I-B and VIII-B family, such as Au, Ag, Pd, and Pt, among others. These elements present the disadvantage of the high cost and low availability in the market. In this sense, this paper presents the doping of ZnO powders with Cu and Ni which are elements of high availability and low cost. The sensing properties of doped ZnO powders were evaluated in the detection of propane gas.

It is worth mentioning that the synthesis route of both pure ZnO and doped ZnO was by the homogeneous precipitation technique, which presents three main advantages, high reproducibility, simplicity, and low cost, since it does not require sophisticated equipment.

2 Experimental procedure

2.1 Synthesis of ZnO samples

Pure and doped ZnO powders were synthesized by the homogeneous precipitation technique. Zinc acetate hydrate ($Zn(CH_3COO)_2{\cdot}2H_2O$, 97%, Sigma Aldrich) at 0.1 M, 0.8159 g of sodium hydroxide (NaOH, 97%, Sigma Aldrich), and 100 ml of ethanol (C_3H_5OH, JT Baker) were used as Zn precursor, precipitating agent, and solvent, respectively. The mixture of these three reagents was heated at 70 °C and then stirred with a magnetic bar at 1200 rpm during 120 min. Nickel nitrate ($Ni(NO_3)$, 99%, Sigma Aldrich) and copper chloride (CuCl, 90%, Sigma

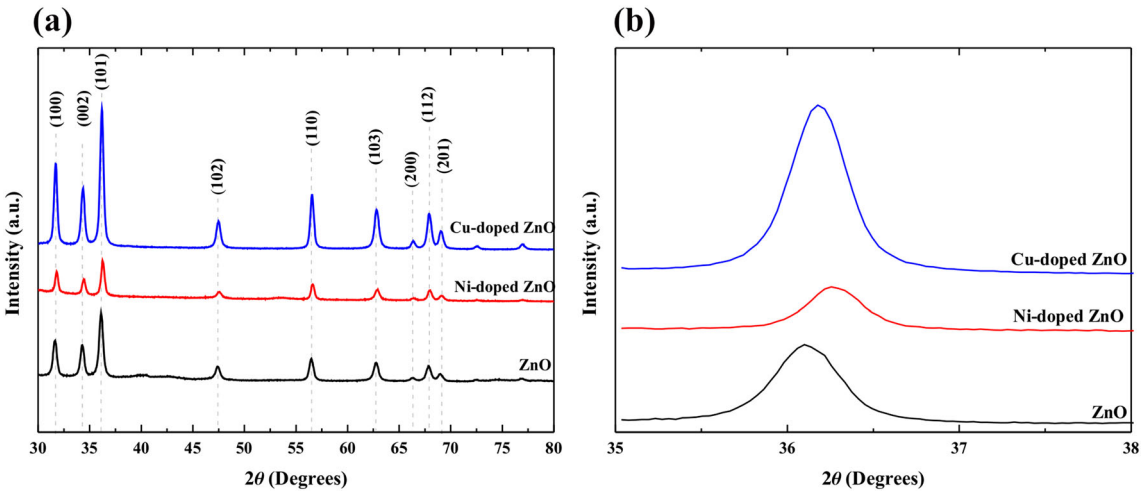

Fig. 1 **a** X-ray diffractograms for all the samples. **b** Close up to (101) peak at $2\theta = 36.21°$

Aldrich) both at 1 at.% were used as dopant precursors of ZnO powders.

The resultant solution was centrifuged at 4500 rpm for 6 min in a centrifuge machine (Eppendorf, Model 5430), and then thrice washed with methanol. Subsequently, the paste obtained was dried in a conventional oven at 100 °C for 1 h and finally dried at 400 °C for 2 h in air atmosphere in order to remove residual organic materials. The sensor pellets with a diameter of 10 mm were manufactured in a mechanical press (ITAL Mexicana) at a pressure of 10 T for 5 min. Two-point ohmic contacts were placed on surface pellets using high-purity silver paint (from SPI).

2.2 Characterization of pure and doped ZnO powders

Chemical composition and crystalline structure were determined by X-ray diffraction by using a X'PERT-PRO diffractometer (PANalytical). The X-ray measurements were carried out by using the Cu-K_α radiation ($\lambda = 1.54060$ Å) and a 2θ angle ranging from 30° to 80°. Elements composition was analyzed by energy-dispersive X-ray spectroscopy (EDS) in all powder samples. Morphological analysis was developed with a AURIGA scanning electron microscope (SEM). The surface area of the pellets (ZnO, ZnO/Ni and ZnO/Cu) was estimated using the BET technique (Brunauer–Emmett–Teller (BET): Micromeritics, Gemini 3240) by 12-point nitrogen adsorption. This analysis was carried out after a degassing process of the pellets at 150 °C for 2 h. Gas sensing characterization consists of measuring the surface electrical resistance of the manufactured pellets placed into a quartz chamber containing propane gas (C_3H_8) at concentrations varying in the 0–500 ppm range at variable operating temperatures, 100, 200, and 300 °C. A Keithley 2001 multimeter was used for electrical resistance measurements, whereas the propane concentration was controlled indirectly with a Leybold Thermovac TM20 vacuum gauge controller.

The gas response estimated from the sensitivities, S, of the pellets was calculated as $S = [R_a - R_g]/R_g$, where R_a is the electrical resistance measured in air and R_g is the resistance measured in a propane gas atmosphere.

3 Results and discussion

3.1 Structural and morphological properties of ZnO powders

Figure 1(a) shows the X-ray diffractograms of pure and Ni and Cu-doped ZnO powders. In all the spectra, nine well-defined peaks are present, which correspond to the hexagonal wurzite-type ZnO structure, according to the JCPDS 01-089-0510 card [26]. The highest intensity peak localized at $2\theta = 36.21°$ is associated with the (101) plane. A low scan of the analysis angle between 35° and 38° allows the observation of a right-slight shift of the (101) peak for doped samples, see Fig. 1b, which is indicative of the incorporation of the dopant elements, Ni and Cu, in the hexagonal zinc oxide lattice. This shift is

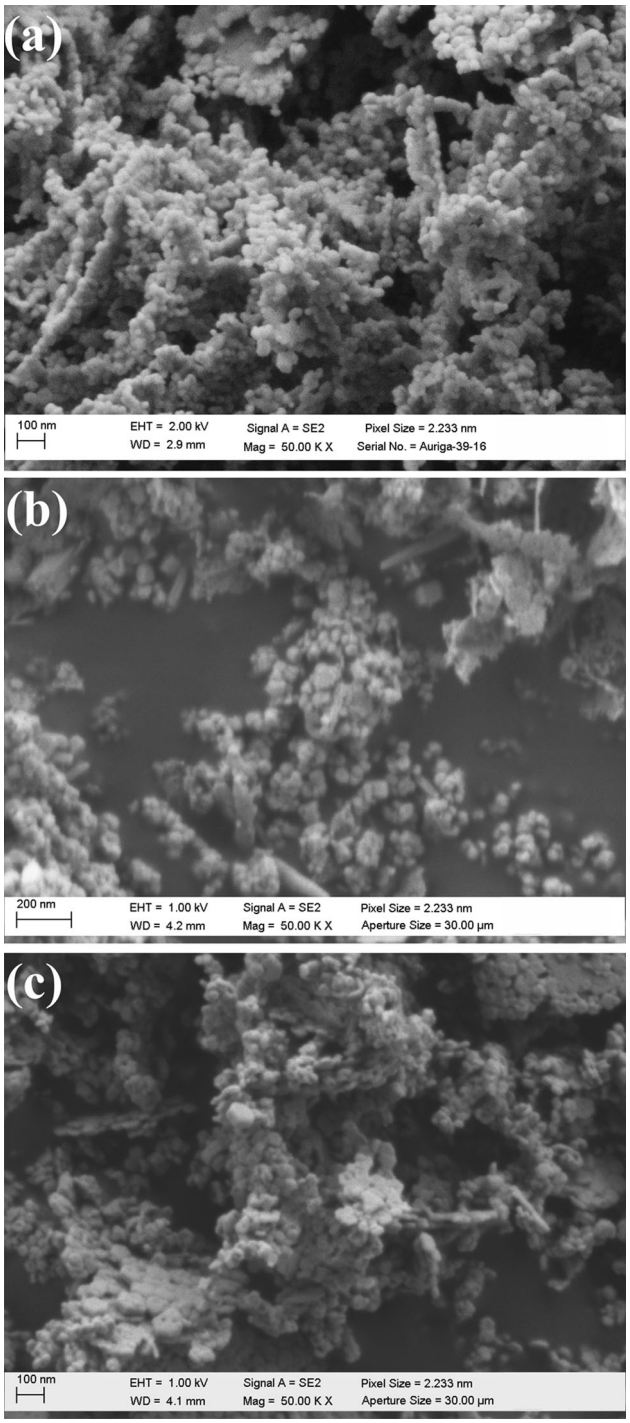

Fig. 2 SEM images of **a** pure ZnO, **b** Ni-doped ZnO, and **c** Cu-doped ZnO samples

attributed to the difference between ionic radius sizes of zinc (0.74 Å) and dopant elements, nickel (0.78 Å) and copper (0.69 Å), producing a slight distortion of the crystal structure due to tension of the lattice.

Table 1 Quantitative analysis of the elements of pure and doped ZnO samples

Elements	ZnO/Ni		ZnO/Cu	
	Wt%	At.%	Wt%	At.%
Zinc	73.73	48.47	65.25	34.12
Oxygen	18.40	49.43	19.89	27.38
Nickel	2.87	2.10	–	–
Cupper	–	–	1.80	0.78

The average crystallite size, D_{hkl}, was calculated using the Scherrer equation:

$$D_{hkl} = c\lambda/\beta\cos\theta,$$

where c is the shape constant (~ 0.89), λ is the wavelength of the Cu-K_α radiation (1.54060 Å), θ is the Bragg angle, and β is the full half-maximum width (FHMW) value of the peak in radians [27]. The full width at half-maximum (FWHM) of the rocking curve peak is taken as a relative measure of the (101) plane. The crystal size for pure ZnO is around the 34.3 ± 0.005 nm, while for the ZnO-doped samples, the crystal size is 37.4 and 37.9 ± 0.005 nm, ZnO/Ni and ZnO/Cu, respectively.

Figure 2 shows SEM micrographs of (a) pure ZnO, (b) Ni-doped ZnO, and (c) Cu-doped ZnO samples. Typical spherical morphology presented in nanostructured semiconductor oxides is observed in the three SEM images; the estimated particle average sizes are 34, 49, and 52 nm, respectively. All samples present similar particle size although the pure ZnO sample shows the formation of more lineal assembles than other two, see Fig. 2a. On the other hand, the Cu-doped ZnO sample suggests morphology with some hexagonal slices, Fig. 2c.

3.2 Energy-Dispersive X-ray analysis (EDX)

The EDX analysis confirms the existence of the elements, Zn, O, Ni, and Cu, in the respective samples, as was expected. The inner insets correspond to the SEM images of the analyzed zone. The carbon detected in the right EDX spectrum comes from the formvar/carbon-coated grid used for this analysis. Table 1 shows the results of the quantitative analysis in atomic percentage of the pure and doped ZnO samples (Fig. 3).

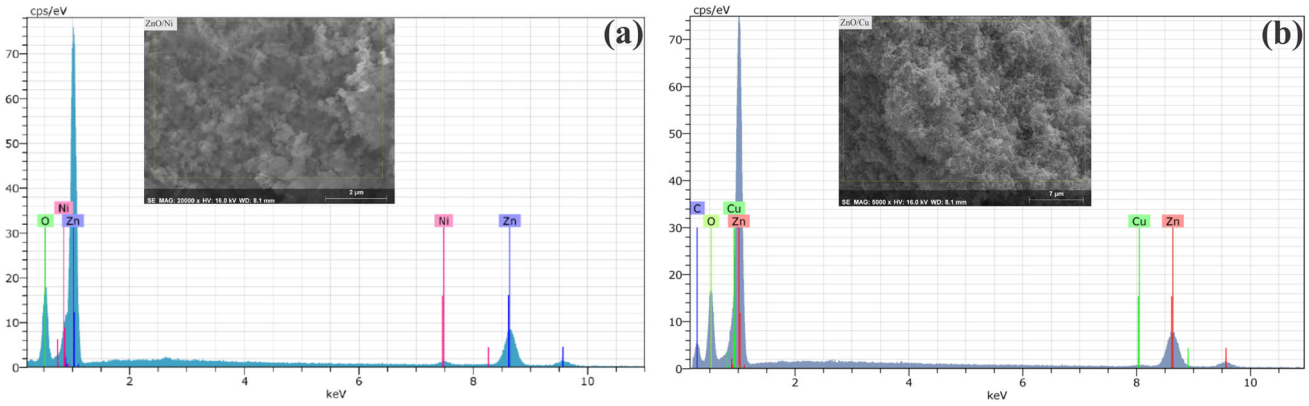

Fig. 3 EDX analysis spectra of **a** Ni-doped ZnO and **b** Cu-doped ZnO samples

Table 2 Surface area and total pore volume of the chemical gas sensors

Sample ID	BET area (m^2/g^{-1})	Total pore volume (m^3/g^{-1})
ZnO	12.50	0.016
ZnO/Ni	13.47	0.023
ZnO/Cu	16.24	0.024

3.3 BET analysis

The surface area and the pore volume in all processed pellets were estimated by using the BET technique. BET analysis results are presented in Table 2. According to the values obtained, the Cu-doped ZnO sampler showed the highest surface area, 16.24 m^2/g^{-1} with a pore volume of 0.024 m^3/g^{-1}.

3.4 Gas sensing properties of ZnO samples

The electrical resistance measurements as a function of the propane concentration and operation temperatures were developed in pellets manufactured from the three different powders, namely, pure and Ni and Cu-doped ZnO; Fig. 4a–c shows these results. It is evident that none sample presented resistance variation at the lowest operation temperature, 100 °C, in all the propane concentrations range used (0–500 ppm), and both pure ZnO and Cu/ZnO pellets neither showed changes at 200 °C, in contrast to Cu-doped ZnO that registered a significant variation around two orders at 200 °C; similar results have been reported in others n-type oxide semiconductors [10].

Measurements carried out at 300 °C and 500 ppm show that all samples present high sensitivity magnitudes, which oscillate from three orders for pure ZnO to five orders in Ni-doped ZnO. Table 3 presents the electrical resistance values measured at 300 °C and different propane concentrations of the three manufactured pellets.

The sensitivity behavior with the operation temperature is directly attributed to the surface chemisorption of the different oxygen species at temperatures between 300 and 450 °C, as has been stated by J. Morales [28] and B. Shohany [29], since the oxygen adsorbed on the sensor surface is more reactive (O^- or O^{2-}) in this temperature range; therefore, the reaction occurring on the surface of the pellets is given as follows: $O^-_{2ads} + e^- = 2O^-_{ads}$, as this increases the temperature [15].

On the other hand, an adsorption mechanism occurs on the ZnO surface when the chemisorbed oxygen species interact with propane gas molecules and these are dissociated and react with the different oxygen species, causing the release of electrons in the band conduction, which in turn decreases the surface potential barrier causing an increase in electrical conductivity [8].

The sensitivity magnitudes of samples measured at 300 °C, estimated by the equation $S = [R_a - R_g]/R_g$, is shown in the plot presented in Fig. 5. Similar to the behavior of the resistance change magnitudes, the maximum responses were obtained at the maximum propane concentration used, 500 ppm, and the maximum sensitivity value was presented in the Cu/ZnO sample. Both doped samples registered a better sensing response than pure ZnO sample. This behavior could be attributed the generation of stress in the film due to the Ni/Zn and Cu/Zn ratio radius, which generates more oxygen vacancies and

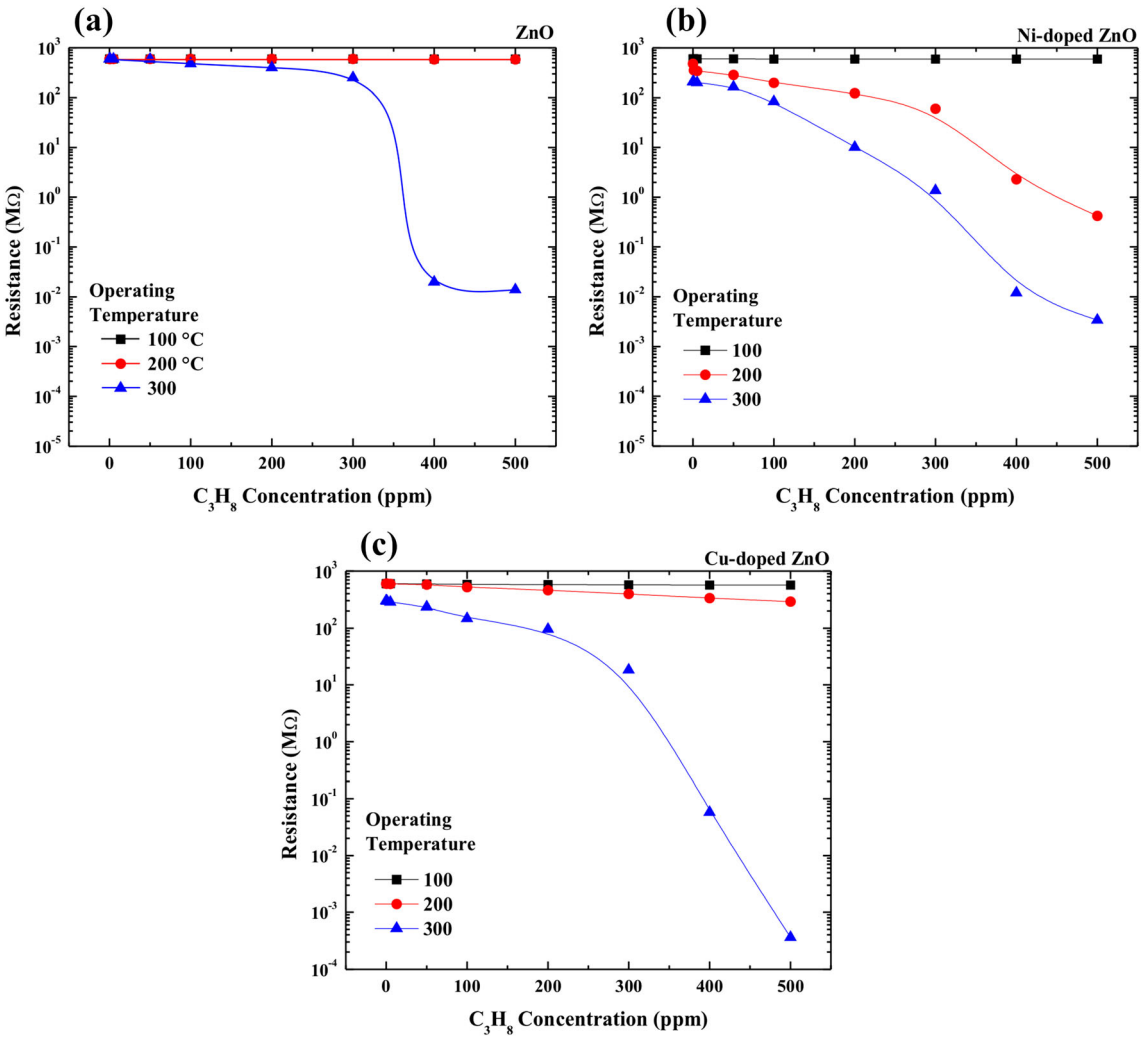

Fig. 4 Graphs of electrical resistance versus propane concentration of **a** pure ZnO, **b** Ni-doped ZnO, **c** Cu-doped ZnO pellets

Table 3 Electric resistance values of pure and Ni and Cu-doped ZnO pellets at different propane concentrations at an operating temperature of 300 °C

Sample ID	Propane gas concentration (ppm)								
	0	1	5	50	100	200	300	400	500
Electric resistance [MΩ]									
ZnO	475	470	338	246	167	87.21	25.36	5.64	1.27
Ni/ZnO	210	207	200	165	84.2	10.14	1.36	0.012	0.0034
Cu/ZnO	300	295	284	236	148	95.6	18.32	0.058	0.00036

interstitial oxygens [30, 31] for adsorbed and increase the sensibility performance. The sensitivity values are reported in Table 4.

4 Conclusion

Semiconductor powders based on pure ZnO, Ni-doped ZnO, and Cu-doped-ZnO were synthesized by the homogeneous precipitation technique. Structural characterization indicated that pure and doped ZnO samples were polycrystalline with a hexagonal wurtzite-type structure. The morphological analysis

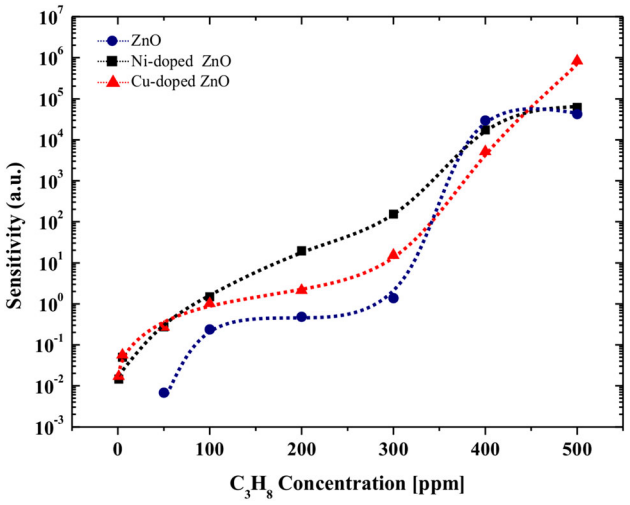

Fig. 5 Sensitivity variation as a function of the propane concentration of the pure ZnO, Ni-doped ZnO, and Cu-doped ZnO samples

Table 4 Sensitivity values calculated from measurements at 500 ppm and 300 °C

Sample ID	C_3H_8 sensitivity
ZnO	4.2×10^4
Ni-doped ZnO	6.1×10^4
Cu-doped ZnO	8.3×10^6

showed that the powders present a small size that is suitable for manufacturing gas sensors, as the area/volume ratio is high. The pellets' sensitivity improved markedly with the doping process. Cu-doped ZnO pellets showed the highest sensitivity, even the Ni-doped ZnO pellets shows an adequate response for an operating temperature of 200 °C.

Acknowledgements

The authors express their gratitude to Adolfo Tavira by the structural characterization (X-ray characterization), the Advanced Laboratory of Electronics Nanoscopy (LANE- CINVESTAV) by the SEM analysis, and Miguel A. Luna by the electrical measurements. R. Herrera acknowledges the postdoc scholarship granted by the Consejo Nacional de Ciencia y Tecnología (CONACyT) – Secretaria de Energía (SENER).

Compliance with ethical standards

Conflict of interest The authors declared that they have no conflicts of interest.

References

1. L. Zhu, W. Zeng, Sensors Actuators A **267**, 242 (2017)
2. A. Díaz, P. Acevedo, P. Aguilar, Sciéndo Ciencia para el Desarrollo **21**, 431 (2018)
3. E. Dilonardo, M. Penza, M. Alvisi, C. Di Franco, F. Malmisano, L. Torsi, N. Cioffi, Beilstein J. Nanotechnol. **7**, 22 (2016)
4. R. Kumar, O. Al-Dossary, G. Kumar, A. Umar, Nano-Micro Lett. **7**(2), 97 (2015)
5. T.-Y. Tseng, Solid State Phenom. **185**, 1 (2012)
6. H.G. Pozos, K.T.V. Krishna, M. de la Luz Olvera Amador, M.Y. Kudriavtsev, A.M. Álvarez, J. Mater. Sci. Mater. Electron. **29**(18), 15829–15837 (2018)
7. J. Morales, A. Maldonado, M. de la L. Olvera, J. Mater. Sci. Mater. Electron. **29**, 15808 (2018)
8. H. Gómez-Pozos, E.J.L. Arredondo, A.M. Álvarez, R. Biswal, Y. Kudriavtsev, J.V. Pérez, Y.L. Casallas-Moreno, M. de la Luz Olvera Amador, Materials **9**(2), 87 (2016)
9. J. Morales-Bautista, A. Maldonado, M. de la L. Olvera, in *12th International Conference on Electrical Engineering, Computing Science and Automatic Control (CCE)*, pp. 1–5 (2015)
10. T.V.K. Karthik, M. De la Luz Olvera, A. Maldonado, H.G. Pozos, Sensors **16**(8), 1283 (2016)
11. H. Guillén-Bonilla, M. Flores-Martínez, V.-M. Rodríguez-Betancourtt, A. Guillen-Bonilla, J. Reyes-Gómez, L. Gildo-Ortiz, M. de la Luz Olvera Amador, J. Santoyo-Salazar, Sensors **16**(2), 177 (2016)
12. J.P. Morán-Lázaro, E.S. Guillen-López, F. López-Urias, E. Muñoz-Sandoval, O. Blanco-Alonso, H. Guillén-Bonilla, A. Guillén-Bonilla, V.M. Rodríguez-Betancourtt, M. Sanchez-Tizapa, M. de la Luz Olvera-Amador, Sensors **18**(3), 701 (2018)
13. K. Schneider, M. Lubecka, A. Czapla, Sensors Actuators B Chem **236**, 970 (2016)
14. A. Rydosz, A. Szkudlarek, Sensors **15**(8), 20069 (2015)
15. M. Abu Haija, A.F.S. Abu-Hani, N. Hamdan, S. Stephen, A.I. Ayesh, J. Alloys Compd. **690**, 461 (2017)
16. L. Zhu, Y. Li, W. Zeng, Appl. Surf. Sci. **427**, 281 (2018)
17. Z.S. Hosseini, A. Irajizad, A. Mortezaali, Sensors Actuators B Chem **207**, 865 (2015)

18. M. Tonezzer, T.T.L. Dang, N. Bazzanella, V.H. Nguyen, S. Iannotta, Sensors Actuators B Chem **220**, 1152 (2015)
19. J. Xu, Z. Xue, N. Qin, Z. Cheng, Q. Xiang, Sensors Actuators B Chem **242**, 148 (2017)
20. D. Zhang, S. Chava, C. Berven, S.K. Lee, R. Devitt, V. Katkanant, Appl. Phys. A **100**, 145 (2010)
21. L. Wang, Y. Kang, X. Liu, S. Zhang, W. Huang, S. Wang, Sensors Actuators B **162**, 237 (2012)
22. X. Wang, X.W. Sun, Y. Yang, C.M.L. Wu, Nanotechnology **20**, 465 (2009)
23. Q. Wan, Q.H. Li, Y.J. Chen, T.H. Wang, X. L. He, J.P. Li, C.L. Lin, Appl. Phys. Lett. **84**, 3654 (2004)
24. V. Galstyan, E. Comini, C. Baratto, G. Faglia, G. Sberveglieri, Ceram. Int. **41**, 14239 (2015)
25. V.V. Ganbavle, S.I. Inamdar, G.L. Agawane, J.H. Kim, K.Y. Rajpure, Chem. Eng. J. **286**, 36 (2016)
26. M. Deshwal, A. Arora, J. Mater. Sci. Mater. Electron. **29**, 15315 (2018)
27. V.K. Jayaraman, A.M. Álvarez, M. de la Luz Olvera Amador, Mater. Lett. **157**, 169 (2015)
28. J.S.J. Hargreaves, Catal. Struct. React. **2**, 1 (2016)
29. B.G. Shohany, L. Motevalizadeh, M.E. Abrishami, J. Theor. Appl. Phys. **12**, 219 (2018)
30. R. Dhahri et al., J. Sci. Adv. Mater. Devices **2**, 34 (2017)
31. S. Ghosh, M. Saha, S.K. De, Nanoscale **6**, 7039 (2014)